Chemical Engineering Journal 411 (2021) 128466

Contents lists available at ScienceDirect

Chemical Engineering Journal

journal homepage: www.elsevier.com/locate/cej

Dual-stage thermosetting photopolymers for advanced manufacturing

Biao Zhang [a,b,*], Ahmad Serjouei [c], Yuan-Fang Zhang [d], Jumiati Wu [d,e], Honggeng Li [d], Dong Wang [f], Hong Yee Low [d,e], Qi Ge [b,*]

[a] Research & Development Institute of Northwestern Polytechnical University in Shenzhen, Xi'an Institute of Flexible Electronics (IFE) and Xi'an Institute of Biomedical Materials & Engineering (IBME), Northwestern Polytechnical University, 127 West Youyi Road, Xi'an 710072, China
[b] Department of Mechanical and Energy Engineering, Southern University of Science and Technology, Shenzhen 518055, China
[c] Department of Engineering, School of Science and Technology, Nottingham Trent University, Nottingham NG11 8NS, United Kingdom
[d] Digital Manufacturing and Design Centre, Singapore University of Technology and Design, 487372, Singapore
[e] Division of Engineering Product Development, Singapore University of Technology and Design, 487372, Singapore
[f] Robotics Institute, School of Mechanical Engineering, Shanghai Jiao Tong University, Shanghai 200240, China

ARTICLE INFO

Keywords:
Dual-stage
Crosslinked photopolymers
Advanced manufacturing
Programmable microstructures
Superhydrophobic

ABSTRACT

We report a dual-stage photocrosslinked polymer network based on sequential ultraviolet (UV)-triggered radical polymerization and thermally activated etherification, applicable to the fabrication of tailorable and programmable high-resolution structures. The first stage involves photoinitiated polymerization of monomer and crosslinker to obtain an intermediate polymer network. As such, sophisticated two-dimensional (2D) and microscale three-dimensional (3D) structures can be made by using UV-based advanced manufacturing technologies. These complex structures can then be readily programmed into other desired, permanent shapes, in the second stage, via thermally triggered etherification which results in a highly crosslinked, robust polymer network. The intermediate network (Stage I) is characterized to have a Young's modulus ranging from 342 to 1146 MPa and a glass transition temperature from 52 °C to 83 °C, depending on the concentration of crosslinker. The same material attains a glass transition temperature ranging from 67 °C to ~105 °C and a Young's modulus of up to 1607 MPa after the subsequent heating process (Stage II). Originally 3D printed 2D structures can be further programmed into rigid, permanent 2.5/3D ones. Micropatterns fabricated from intrinsically hydrophilic dual-stage crosslinked photopolymers through soft lithography show superhydrophobicity, and can subsequently be molded with different curvatures for practical applications.

1. Introduction

Photocrosslinked polymers are the polymers which transfer liquid resins into solid covalent-crosslinked polymeric materials when exposed to visible or ultraviolet (UV) light in the presence of photoinitiators [1–4]. Photocrosslinked polymers show great advantages in terms of the fast-crosslinking rate, as the transition from liquid to solid can be realized within a few minutes or even seconds, as well as the temporal and spatial controls during the photopolymerization process [1–4]. Due to these outstanding properties, photopolymers have been used in dentistry [5], tissue engineering [6–8], electronic materials [9], optical materials [10,11], coatings and surface modifications [12–14], and other fields [15].

Recently, there has been an increasing interest in associating photopolymers with advanced manufacturing technologies such as three-dimensional (3D) printing and imprint lithography which benefit a variety of application fields such as actuators, grippers, and device patterning [16–19]. However, once the structures are generated by 3D printing or imprint lithography, they do not have malleability and cannot be reprogrammed to another shape since the chemically crosslinked 3D networks are permanently formed through photopolymerization.

In this regard, dual-stage polymerization which generates stable materials via two curing stages with the application of different stimuli (i.e. UV or thermal exposure) offers higher manufacturing flexibility, and a possible solution to address the aforementioned challenge [10]. Click reactions have been widely employed to develop dual-stage photopolymerization polymers because of their simplicity and eco-friendly

* Corresponding authors at: Research & Development Institute of Northwestern Polytechnical University in Shenzhen, Xi'an Institute of Flexible Electronics (IFE) and Xi'an Institute of Biomedical Materials & Engineering (IBME), Northwestern Polytechnical University, 127 West Youyi Road, Xi'an 710072, China (B. Zhang).
E-mail addresses: iambzhang@nwpu.edu.cn (B. Zhang), geq@sustech.edu.cn (Q. Ge).

https://doi.org/10.1016/j.cej.2021.128466
Received 2 October 2020; Received in revised form 23 December 2020; Accepted 6 January 2021
Available online 12 January 2021
1385-8947/

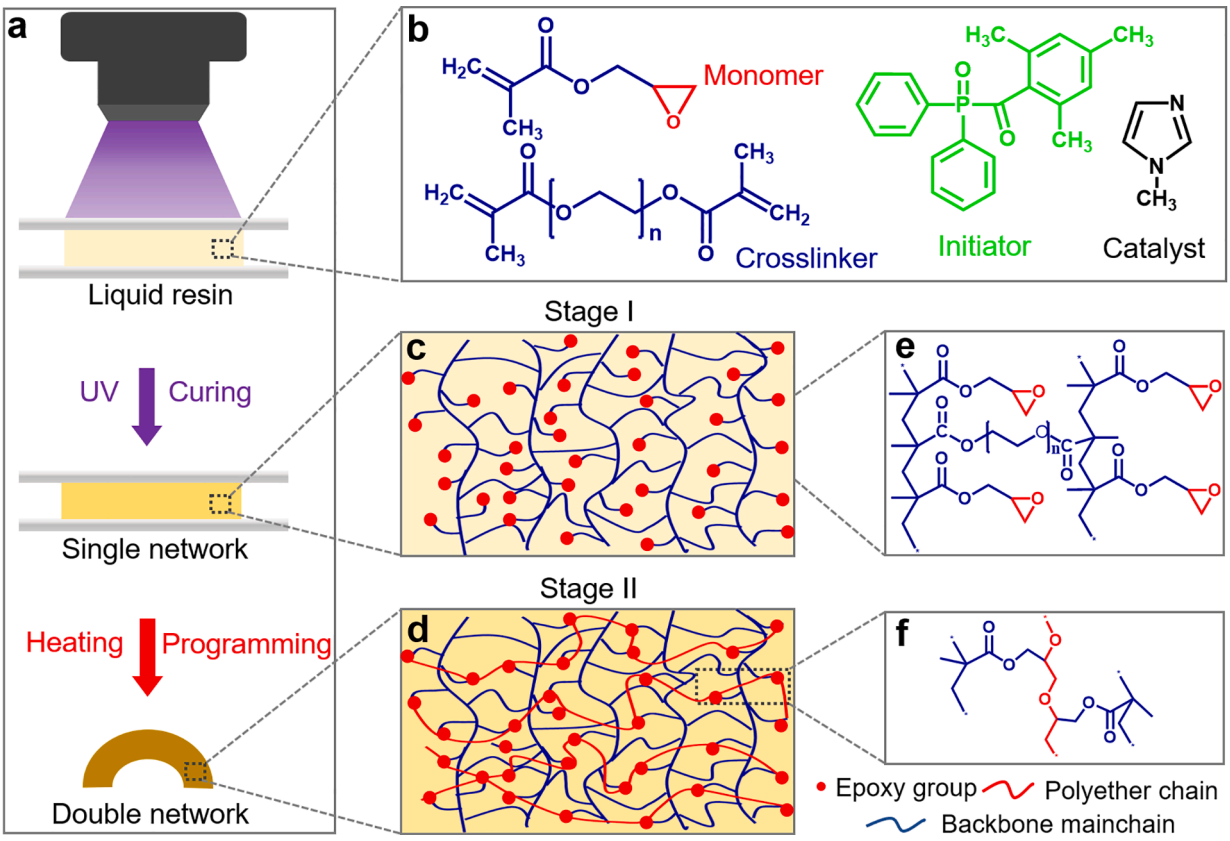

Fig. 1. Synthesis methodology of dual-curing polymer network systems. (a) Schematic illustration of the dual-curing process. (b) Chemical structures of monomer (glycidyl methacrylate, GMA), crosslinker (poly(ethylene glycol) dimethacrylate (Mn = 550 g/mol), PEGDMA), initiator (diphenyl(2,4,6-trimethylbenzoly) phosphine oxide, TPO), and catalyst (1-Methylimidazole) used in this study. (c) The crosslinked network formed in Stage I. (d) The crosslinked network formed in Stage II. (e) The detailed chemical network of Stage I. (f) The detailed chemical network of Stage II.

nature. For example, thermally triggered click reactions, such as thiol-Michael addition, thiol-epoxy, or aza-Michael addition, have been combined with UV or thermally initiated polymerization [20–25] to form two-step curing systems which have been applied to impression materials [10], shape memory materials [20] and holograms [23]. The advanced manufacturing technologies such as 3D printing and imprint lithography benefit from the dual-stage polymerization if it follows the polymerization sequence from UV curing to thermal curing where the first UV curing stage was used to form the designed shape of fabricated structure; the second thermal curing stage offered the fabricated structure higher mechanical property, and the capability of reprogramming to another shape [26–34]. Griffini and coworkers [31] introduced a dual-curing interpenetrating polymer network (IPN) system obtained by mixing a UV-curable acrylic monomer with a thermally reactive epoxy resin for UV-assisted direct ink writing (DIW). The mechanical performance of the printed structures was enhanced by a thermal treatment that followed. In addition, this dual-curing formulation was used to fabricate carbon-fiber reinforced (CFR) composites. Cushen and coworkers [32] invented epoxy dual-curing resins for 3D printing. In their work, an intermediate 3D object was formed with resin exposed to light, which was further cured with sufficient heating and/or microwave irradiation. Qi and coworkers [33] also reported a hybrid ink containing both photocurable resin and thermally curable epoxy resin, which was used to realize high-speed printing of high-performance thermosets via two-stage curing. Besides, dual-cure benzoxazine networks [34], dual-curing acrylate-isocyanate ester system [35] and dual-curing resin with cationic curable vegetable oil [36] have also been used in 3D printing. The main purpose of introducing the second stage curing is to improve the mechanical and thermal properties of printed thermosets [37]. Besides, two-step 3D printing approach has also been used in constructing thermosets with shape-memory properties [38,39]. However, even the network buildup process during the first curing stage allows tailoring the structure and properties of the intermediate materials [10,20,23], there are seldom works that combine this property of dual stage materials with advanced manufacturing. Recently, Zhang et al. reported a two-step polymerization strategy to develop 3D printable reprocessable thermosets (3DPRTs) that allow users to reform a printed 3D structure into a new arbitrary shape [40]. However, the relatively low glass transition temperature (~55 °C) and room temperature modulus (900 MPa) constrain the 3DPRTs from practical applications.

In this work, we report a dual-stage photopolymer system based on synthesis of an epoxy functional methacrylate resin in two sequential stages of, respectively, photo-activated radical polymerization and thermally activated etherification (Fig. 1a). In the first stage (Stage I), sophisticated two-dimensional (2D) patterns and micro-scale 3D structures were made by UV-based advanced manufacturing technologies, such as digital light processing (DLP) and imprint lithography [19]. In the second stage (Stage II), the complex structures obtained could be easily programmed into other desired shapes by thermally triggered curing. In Stage II, a highly crosslinked, robust polymer network with glass transition temperature ranging from 67 to 100 °C was formed, allowing the structures to permanently maintain their shapes. Factors such as the curing time, the stability of the epoxy group and the effect of the catalyst during the photopolymerization in Stage I were studied. Effects of the concentration of catalyst and the processing temperature on the mechanical performance of material in Stage II were investigated as well. The final mechanical properties of the polymer system were shown to be dependent on the proportions of monomer and crosslinker with a glass transition temperature ranging from 67 °C to ~105 °C and a

Young's modulus of up to 1607 MPa. 2D structures made of this dual-curing polymer network were demonstrated to be programmable into rigid, permanent 2.5/3D ones. Furthermore, superhydrophobicity was discovered for micropatterns fabricated from the intrinsically hydrophilic material. Substrates with such patterns obtained from Stage I could be molded with desired curvatures in Stage II for practical applications.

2. Materials and methods

2.1. Materials

Glycidyl methacrylate, poly(ethylene glycol) dimethacrylate (Mn = 550 g/mol), Sudan I, diphenyl(2,4,6-trimethylbenzoly) phosphine oxide and 1-Methyimidazole were purchased from Sigma-Aldrich (Singapore) and used as received.

2.2. Preparation of samples

Solutions were prepared by mixing Glycidyl methacrylate as monomer and poly(ethylene glycol) dimethacrylate as crosslinker in different concentrations and adding diphenyl(2,4,6-trimethylbenzoly) phosphine oxide as initiator (5 wt% of total amount of monomer and crosslinker) and 1-Methylimidazole as catalyst in different concentrations. The prepared inks are stable for more than 1 month when stored in amber laboratory bottles at −20 °C, which can be used directly for printing (Fig. S1). Solutions were then poured into a Teflon mold with dimensions of 50 mm × 50 mm × 0.5 mm (length × width × thickness) which was covered with thin transparent Teflon films. A Stage I film sample was obtained by shining UV light of 365 nm wavelength on the mold in a UV-oven (UVP, Ultraviolet Crosslinkers, Upland, CA, USA) for 10 min. The film was removed from the mold and manually cut into strips of desired dimensions for simple tension and Dynamic Mechanical Analysis (DMA) tests. Stage II samples were obtained by putting the Stage I strip samples into a Memmert U universal heating oven (Germany) for thermal treatment at the desired temperature.

In the following sections, the sample nomenclature will be further defined as GxPy, where G and P represent glycidyl methacrylate (GMA) and poly(ethylene glycol) dimethacrylate, while × and y correspond to the weight concentrations of GMA and PEGDMA, respectively.

2.3. Preparation of solutions for 3D printing

The solutions for 3D printing were prepared by adding Sudan I (0.02 wt% of the total weight) as photoabsorber to the solutions used for aforementioned sample preparation. All the solutions were degassed under vacuum before use.

2.4. Fourier Transform Infrared Spectroscopy (FTIR)

Fourier Transform Infrared Spectroscopy (FT-IR) results were recorded using ATR mode with a Magna-IR Nicolet 550 collecting 32 scans from 400 to 4000 cm^{-1}.

2.5. Dynamic Mechanical Analysis (DMA)

DMA experiments were performed in the tension film mode on strip specimens with dimensions of 15 mm × 3.5 mm × 0.5 mm (gauge length × width × thickness) with a TA Instruments Q800 DMA tester. The sample temperature was increased from 0 to 150 °C at a ramp rate of 3 °C min^{-1}. The frequency was 1 Hz and the amplitude was 5 μm. The glass transition temperature (T_g) is determined as the temperature at which the tanδ curve reaches its maximum.

2.6. Simple tension test

Simple tension experiments on strip specimens with dimensions of 15 mm × 5 mm × 0.5 mm (gauge length × width × thickness) were conducted using a TA ElectroForce 3230-ES mechanical testing machine with a 450 N load cell at a strain rate of 0.01 s^{-1}. Simple tension test at high temperature for each material composition (for both Stage I and II samples) was performed at the specific temperature corresponding to the minimum storage modulus of Stage I sample in DMA results to eliminate the effect of thermally triggered etherification. Young's modulus was measured as the initial slope of the material stress-strain curve in the linear regime.

2.7. 3D printing

The prepared UV-curable solutions were photopolymerized by Digital Light Processing (DLP) method [41]. A customized micro-stereolithography system with a 405-nm wavelength light source was used in this study. 3D models of structures in STL format were first sliced into layers with the target thickness. Next, the printing parameters were set with a LabVIEW program. The structures were printed with layer-by-layer exposure to UV light. After printing, the extra solution on the surface of the obtained 3D structures was removed by blowing air with a rubber suction bulb. Finally, the structures were post-cured in a UV oven (wavelength: 365 nm, UVP, Ultraviolet Crosslinkers, Upland, CA, USA) for no less than 10 min to make sure all the methacrylate groups have been consumed (Fig. S2).

2.8. Imprint lithography

High resolution and well-defined surface textures can be precisely fabricated through imprint lithography. Silicon molds were cleaned using Piranha solution (a 3:1 mixture of 96% sulfuric acid with 30% hydrogen peroxide) at 120 °C for 30 min, rinsed with deionized water, dried in a stream of dry nitrogen and kept in a clean oven at 100 °C for 1 h. The molds were further treated with a fluorosilane release agent (0.1 mL) for 4 h by vapour deposition of 1H, 1H, 2H, 2H-perfluorodecyltrichlorosilane self-assembled monolayer. This is to ensure that there is no influence of silane on the subsequent contact angle measurements. The prepared UV curable solution was then poured into the treated silicon molds and cured for 10 s under UV light (wavelength: 265 nm). Patterns were formed upon demolding.

2.9. Water contact angle measurement

Wettability of samples was characterized by measuring the static water contact angles (CAs) using a sessile drop method on a contact angle goniometer (Kino SL200KS). A deionized water droplet (4 μL) was dispensed gently onto the sample surface using a motorized micro-syringe, and a photograph of the water droplet was taken immediately by the goniometer camera. CA values were obtained from the integrated software in the goniometer. For every stretched sample batch (n = 3), at least 5 measurements were conducted at the center of the neck region to give an average value of contact angle in each of two directions: perpendicular to and parallel with the stretching direction.

3. Results and discussion

3.1. Preparation of the dual-curing polymer system

To make the dual-curing polymer system suitable for UV-based manufacturing technologies such as Digital Light Processing (DLP) based 3D printing and imprint lithography, the first curing stage should be photo-triggered. Based on this principle, we chose glycidyl methacrylate (GMA) as the monomer, poly(ethylene glycol) dimethacrylate (PEGDMA) as the crosslinker and diphenyl(2,4,6-trimethylbenzoly)

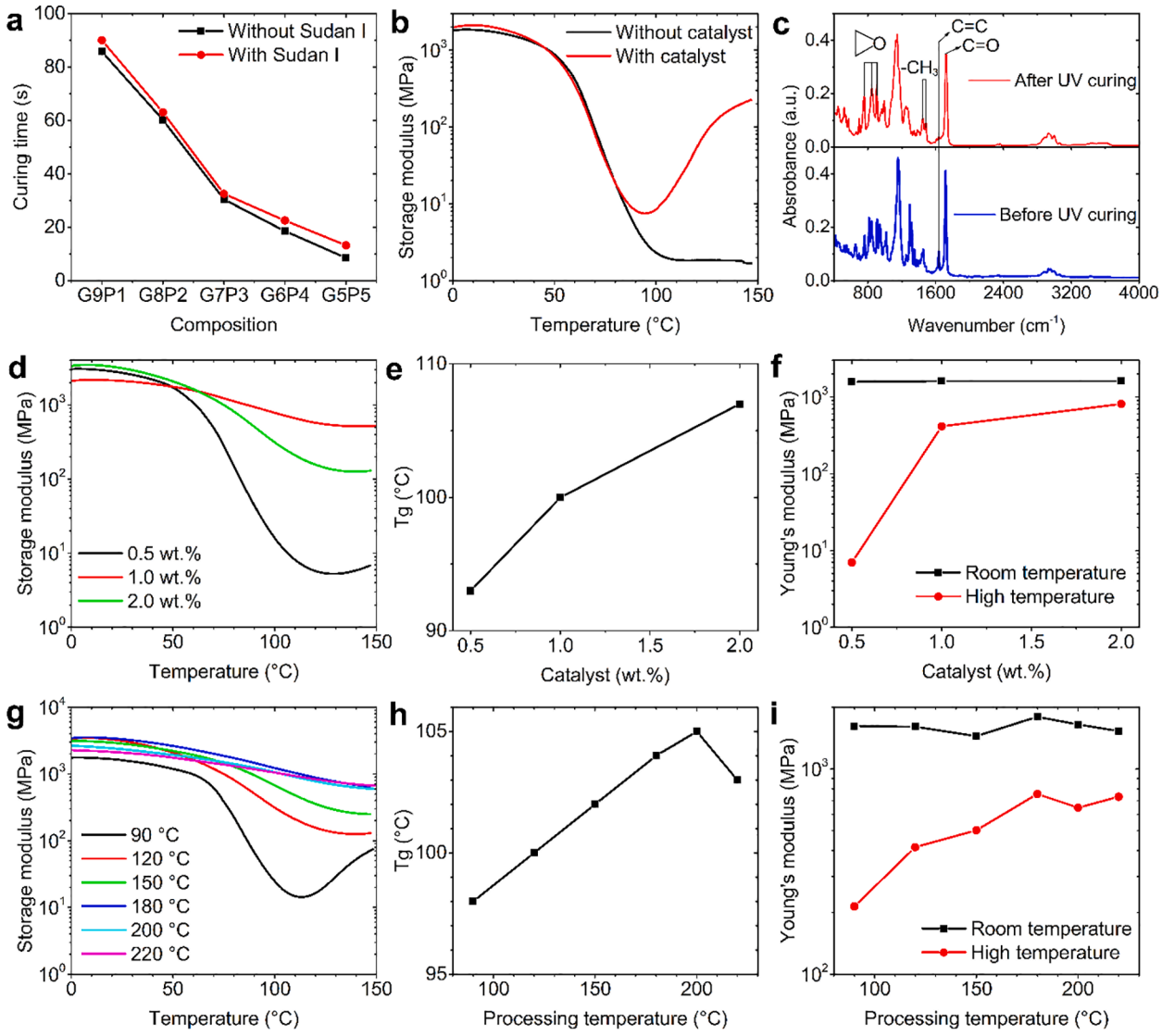

Fig. 2. The performance of UV-triggered photopolymerization in Stage I and thermal treatment in Stage II. (a) The curing time as a function of polymer resin composition and the effect of the absorber (Sudan I, 0.02 wt%). G represents Glycidyl methacrylate (GMA); P represents poly(ethylene glycol) dimethacrylate. The concentration of the initiator is 5 wt% of the total weight of monomer and crosslinker. The light source has a wavelength of 405 nm. (b) Dynamic Mechanical Analysis (DMA) results of materials formed by curing the mixtures of GMA and PEGDMA (9/1 w/w) with and without catalyst (1-methylimidazole, 1 wt% of the total weight of monomer and crosslinker) under UV light for 10 min. (c) Infrared spectra of the liquid resin composed of GMA and PEGDMA (9/1 w/w) with catalyst (1-methylimidazole, 1 wt% of the total weight of monomer and crosslinker) and initiator (5 wt% of the total weight of monomer and crosslinker) (red) and the corresponding photopolymerized network (black, under UV light for 10 min). (d-i) The mechanical performance of the thermally treated materials obtained from UV-cured mixtures of GMA and PEGDMA (9/1 w/w). (d) DMA curves, (e) The glass transition temperature (T_g), and (f) Young's modulus (at 30 °C and 90 °C) as functions of the concentration of catalyst. All the materials were heated at 120 °C for 1 h. (g) DMA curves, (h) The glass transition temperature (T_g), and (i) Young's modulus (at 30 °C and 90 °C) as functions of the processing temperature. All the materials contained 1 wt% of catalyst and were heated for 1 h.

phosphine oxide (TPO) as the photoinitiator to constitute the liquid resin (as shown in Fig. 1b). In addition, 1-Methylimidazole was added as the catalyst of etherification. As demonstrated in Fig. 1c, a crosslinked network is obtained after UV-triggered polymerization of monomer and crosslinker solution, and the crosslinked network in stage I is from the opening of the double bonds on difunctional dimethacrylate groups of crosslinker (Fig. 1e). Next, the density of crosslinked network increases upon heating (Fig. 1d) in Stage II due to etherification (Fig. 1f). The UV-active methacrylate groups allow the materials to be printed in high resolution and complex geometries by advanced manufacturing. The epoxy group in glycidyl methacrylate provides the printed structures with the potential to be further cured by heating (Fig. S3).

3.2. Study of UV-trigger photopolymerization in Stage I

The curing time, an important parameter in 3D printing, was studied by varying the proportions of monomer and crosslinker in the resin. As shown in Fig. 2a, the curing time decreases with increasing crosslinker (PEGDMA) concentration. The time required for curing a 140-μm-thick layer is 87 s when the resin contains 10 wt% of PEGDMA, while this value is reduced to 8.5 s for the resin with 50 wt% of PEGDMA. Moreover, the addition of dyes, which can improve the printing resolution [42,43] also affects the curing time of the resin (Fig. 2a). Adding 0.02 wt % of Sudan I causes the time to cure a single layer to increase by 3 ~ 5 s irrespective of the resin composition. To avoid the impact of the reaction conversion of first stage curing on the second stage curing, all the samples from Stage I were cured under UV oven for at least 10 min (Fig. S2).

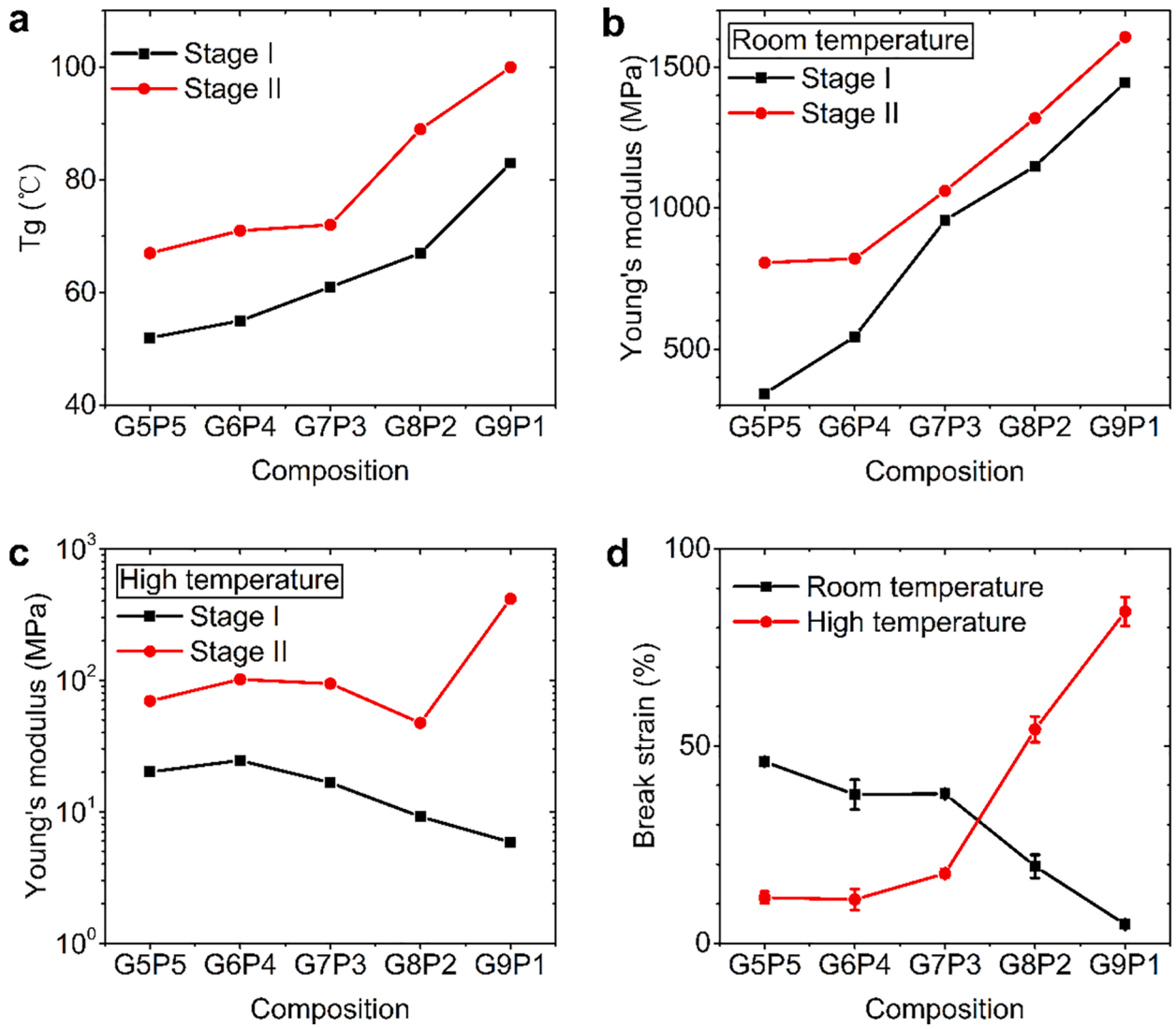

Fig. 3. Comparison of mechanical performance between materials in Stages I and II. (a) The glass transition temperature (T_g) calculated from DMA results (Figs. S8 and S9); (b) Young's modulus at room temperature (30 °C); (c) Young's modulus at high temperature, and (d) failure strain (at room and high temperatures) as functions of material composition. G stands for Glycidyl methacrylate (GMA) and P, poly(ethylene glycol) dimethacrylate.

Despite the role of 1-Methylimidazole as the catalyst for the thermally triggered etherification[44] in Stage II, it may also have an influence on the photopolymerization in Stage I. To investigate this, we compared the dynamic mechanical analysis (DMA) curves of materials from UV-cured liquid resins with and without catalyst (Fig. 2b). The addition of catalyst does not significantly affect the storage modulus within the temperature range from 0 °C to 80 °C. However, for higher temperatures, the storage modulus is considerably greater for materials with catalyst than those without it. This phenomenon can be attributed to the catalyzed etherification at high temperature (>80 °C).

As the epoxy group is key to the thermally triggered etherification, we studied its stability during the UV-curing process by Fourier transform Infrared Spectroscopy (FT-IR). Fig. 2c shows the infrared spectra of absorption of the liquid resin and the corresponding polymer network obtained after 10 min of photopolymerization. There is, in both spectra, a strong absorption band at 1726 cm^{-1} which can be induced by the stretching of ester group. As the ester group did not participate in the UV-triggered polymerization, this peak was used to normalize the two spectra. After UV-curing, the absorption band at 1600 cm^{-1} attributed to C═C group almost disappeared, suggesting nearly complete consumption of the monomers and crosslinkers. Meanwhile, the absorption bands attributed to the pendant epoxy functional group at 755, 843, 905, and 1253 cm^{-1} do not show apparent attenuation, thus demonstrating the stability of the epoxy group during photopolymerization. Overall, addition of catalyst and longtime UV-curing (no less than 10 min) do not affect the stability of the epoxy group.

3.3. Study of thermal treatment in Stage II

3.3.1. Effects of processing conditions

The mechanical performance of the thermally processed materials originating from the dual-curing polymer system could be affected by several parameters, among which the concentration of catalyst and the processing temperature are the most important.

We investigated the effect of the concentration of catalyst on samples that, after UV-curing, underwent thermal treatment at 120 °C for 1 h. The concentration was varied from 0.5 wt% to 2.0 wt%. Fig. 2d shows the changes in storage modulus of the processed samples as a function of temperature. The storage modulus increases with increasing concentration of catalyst at high temperature. With 0.5 wt% of catalyst, the etherification reaction is incomplete between 120 °C and 150 °C as indicated by an upturn in storage modulus. For the same increase in concentration of catalyst, the glass transition temperature (T_g), determined by the peak of tanδ measured in DMA tests, shifts from 93 °C to

Fig. 4. 3D printing of dual-curing polymer network system. (a) Scheme of DLP apparatus. (b) Demonstration of printed structures. The scale bars all represent 2.0 mm. (c, d) Examples of programming printed 2D sheets into permanent 2.5/3D structures through dual-stage processing.

107 °C (Fig. 2e). The Young's modulus at room temperature, calculated from uniaxial tensile test results, is not affected by the concentration of catalyst (Fig. 2f). Nonetheless, the Young's modulus rises dramatically from 7 MPa to 813 MPa at a high temperature set as 90 °C.

Mechanical properties of thermally treated materials were also tested for different processing temperatures ranging from 90 °C to 220 °C while keeping the concentration of catalyst at 1.0 wt% and the processing time at 1 h. As shown in Fig. 2g, the storage modulus gradually increases with increasing processing temperature from 90 °C to 180 °C. The upturn in storage modulus at high temperature for the sample processed at 90 °C in Fig. 2g and a similar behavior observed for 0.5 wt% of catalyst in Fig. 2d, could also be explained by the incompleteness of etherification reaction. When we further increase the processing temperature from 180 °C to 220 °C, no apparent increase in rubbery modulus is observed, indicating an equilibrium state has been reached. Similarly, the glass transition temperatures (T_g) increased from 98 °C to ~105 °C with the same increase in processing temperature and were eventually stable at ~105 °C (Fig. 2h). The shift in T_g does not affect the Young's modulus of material at room temperature but rather at high temperature, here set as 90 °C, where the value changes from 214 MPa to ~750 MPa (Fig. 2i). In addition, we further prolonged the treatment time from 1 h to 2 h with the processing temperature from 180 °C, to 200 °C and 220 °C, respectively. As shown in Fig. S4, the storage modulus curves are almost re-combined, demonstrating that the materials properties reached a stable state when the post treatment condition was set as 1 h at 180 °C. Further prolonged treatment time or higher treatment temperature would not change the final properties of materials. More detailed information is provided in Table S1.

3.3.2. *Effects of material composition*

Fig. 3a summarizes the T_g values of materials with various proportions of monomer and crosslinker in Stages I and II. The T_g of Stage I networks varies from 83 °C to 52 °C with an increase in crosslinker concentration from 10 wt% to 50 wt%. As the T_g of the pure polymers from PEGDMA550 and GMA are ~4.7 °C and 88 °C (Fig. S5, Fig. S6 and Table S1), respectively, which indicated that molecular chains from GMA are more rigid than from PEGDMA, we speculate that the decrease of T_g with increasing amount of PEGDMA in GxPy system is due to the flexibility of PEGDMA molecular chains [45]. Moreover, as shown in Fig. S7, GxPy system is found to be fit for Couchman equation [46], which can be used to guide material design with a desired T_g by mixing the GMA and PEGDMA with prescribed ratios: $1/T_g = M1/T_g^1 + M2/T_g^2$. Here, T_g^1 and T_g^2 are the glass transition temperatures of the respective pure-components, and M1 and M2 are the corresponding mass fractions. The T_g in Stage II shows a similar tendency, decreasing from 100 °C to 67 °C with the same increase in crosslinker concentration. More specifically, for a given crosslinker concentration, the T_g increases by 15 ~ 20 °C after heating, i.e. from Stage I to Stage II, which might be attributed to thermally triggered etherification introducing additional crosslinks that restrict segmental chain mobility, and therefore results in the increase in T_g at Stage II [47–49]. As a reference for comparison, the T_g of homopolymer from polymerization of PEGDMA (PPEGDMA) shifts by merely 5 °C after heating (Fig. S5).

The effect of material composition on the Young's moduli is shown in both Fig. 3b and c, respectively for uniaxial tensile tests at room temperature and the specific high temperature at which the storage modulus is minimum in DMA results of Stage I sample to eliminate the effect of etherification triggered by heating. As shown in Fig. 3b, the Young's modulus at room temperature increases with decreasing PEGDMA concentration. The Young's modulus of this dual-curing polymer network system in Stage I spans from 1146 MPa to 342 MPa at room temperature with the crosslinker concentration varying from 10 wt% to 50 wt%. In comparison, the same material can attain a Young's modulus ranging from 1607 MPa to 807 MPa at room temperature after the subsequent post-curing, hence demonstrating an improved mechanical performance. Likewise, at high temperature (Fig. 3c), the post-heated material (Stage II) also has a higher Young's modulus than the same material network obtained from photopolymerization (Stage I).

The failure strain is another critical material property especially for shape programming as it dictates the capability of structure deformation and/or actuation [50]. Fig. 3d shows the failure strain of Stage I materials as a function of material composition at both room temperature and relatively high temperatures. Homopolymer PPEGDMA, which has a very low break strain (~5%) at room temperature (30 °C), was used as a reference for comparison. UV-curing of a resin mixture with 50 wt% of PEGDMA and 50 wt% of GMA yields a material with failure strain of 45% at room temperature. As the proportion of GMA is further increased, this value gradually decreases to as low as ~3% (G9P1: 10 wt % of PEGDMA and 90 wt% of GMA). As molecular chains from GMA are more rigid than from PEGDMA (Figs. S5 and S6), and considering the resulting decrease of T_g with increasing amount of PEGDMA in GxPy system, we believe that the increase of the rigidity of molecular chains hindered extended segment during stretching, resulting in brittle

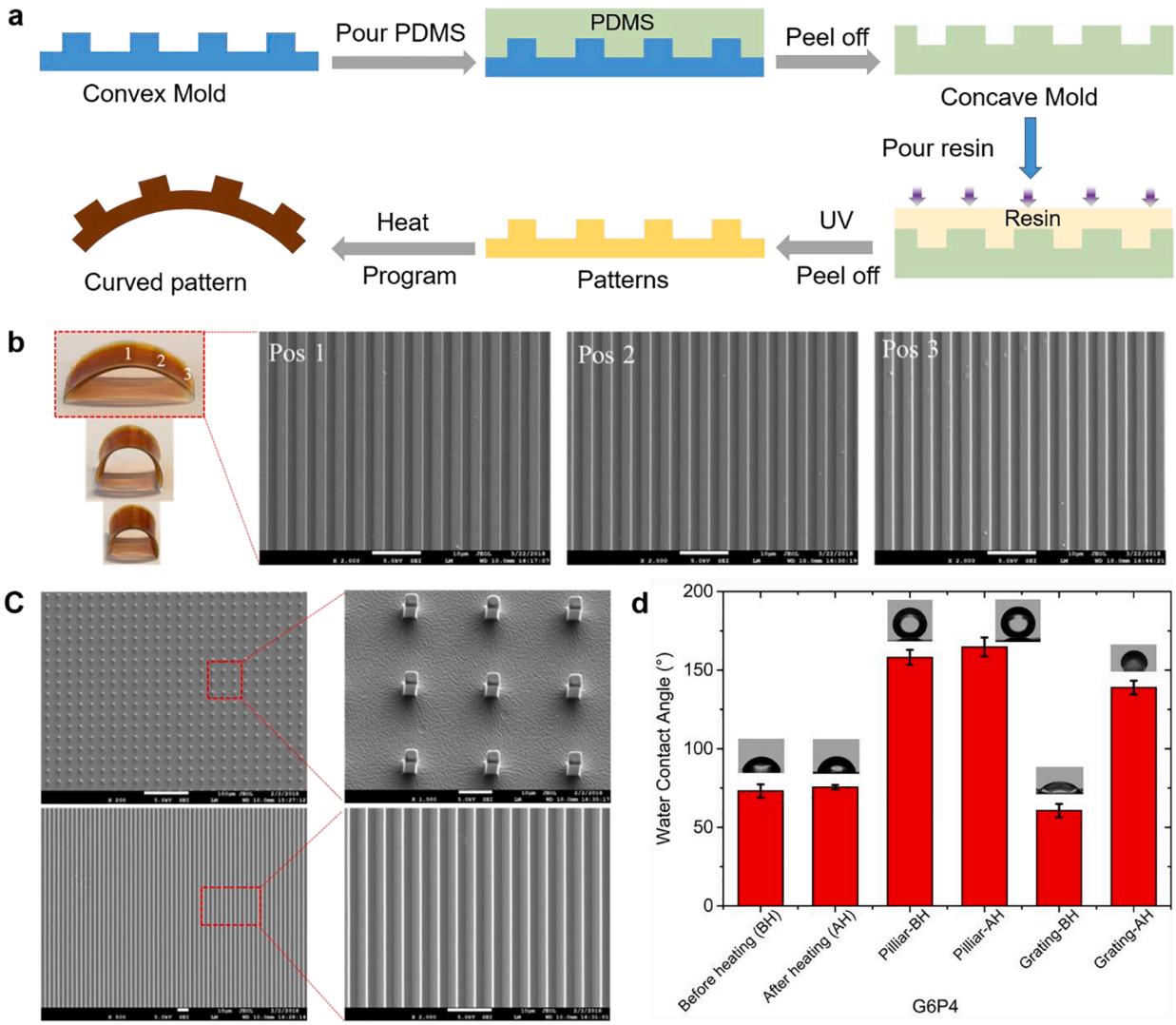

Fig. 5. Imprinting of dual-curing polymer network system. (a) Schematic demonstration of the imprinting process. (b) Snapshots of curved micropatterns with different curvatures (R = 4.5 mm, to 5.5 mm and 10 mm) and SEM images of the surface with grating patterns in three different positions. (c) SEM micrographs of fabricated micropatterns at different scales. (d) Influence of the fabricated micropatterns on the water contact angle (WCA) with their corresponding WCA images as insets. The used material is composed of GMA and PEGDMA at 6/4 (w/w).

fracture. Conversely, the failure strain increases from 12% to 82% when the concentration of GMA is augmented from 50% to 90% at high temperature. At high temperature, materials are under rubbery state and the increase of the proportion of GMA leads to the decrease of cross-linker concentration of GxPy system, and thus the increase of break strain [48,49]. These results could provide guidance on the choice of temperature for shape programming. More detailed information on the mechanical performance of the dual-curing polymer network system is provided in Fig. S10 and Table S2, respectively.

3.4. *Examples of applications*

3.4.1. *3D printing*

The photo-triggered polymerization in Stage I makes the dual-curing polymer network system suitable for UV-based 3D printing technologies, such as Digital Light Processing (DLP) based 3D printing technology (Fig. 4a). Fig. 4b demonstrates several structures which were printed from the dual-curing polymer network system with our customized UV-based 3D printing apparatus [19]. Furthermore, benefiting from the UV-activity of the proposed dual-curing polymer network system, we can easily create 2.5/3D structures from flat (2D) photopolymerized structures, thus reducing the fabrication time. As shown in Fig. 4c and d, we first printed 2D sheets by DLP that can be further programmed into other desired shapes at high temperature. The new shapes become final after a thermal treatment. Three examples are shown: a printed flat sheet showing the letters “SUTD” was bent into a free-standing shape; a printed 2D lattice structure was rolled into a bracelet shape; and a printed 2D configuration containing the separate letters in the “SUTD” logo was programmed into a 3D box with the logo letters forming the sidewalls. Obtaining these programmed structures with the reported technique requires considerably less time than directly printing them out in the final 3D geometries. Being stable even at higher temperatures, the thermally processed structured are suitable for use in harsh environments. Additionally, this dual-curing polymer system shows no apparent shrinkage during heating (0.58%, Fig. S11), which is a highly desirable characteristic in manufacturing. This method offers a facile and convenient way to fabricate functional microstructures, *e.g.* as tools for microfluidic dynamic study [51].

3.4.2. *Soft-lithography*

Inspired by nature, an increasing number of biomimetic surfaces in micro-scale, which exhibit superhydrophobic properties, have been successfully engineered [52–55]. Micro- and nanoscale surface topographies that give rise to superhydrophobic surfaces have been achieved

mostly on 2-dimensional planar objects [56,57]. Recently, increasing interests in superhydrophobic surfaces on consumer products, optics, and biomedical devices demand topographic patterning on freeform nonplanar surfaces [58–60]. The low viscosity and UV curable properties make our dual-stage thermosetting photopolymer system suitable for imprinting technique to fabricate micropatterns. Moreover, the formed micropatterns can be bent to the desired curved shapes with strengthened mechanical performance. As shown in Fig. 5a, high resolution and well-defined surface textures can be precisely fabricated through imprint lithography (Detailed fabrication process can be seen in *Materials and Methods section*). Fig. 5b shows substrates with micropatterns obtained from Stage I could be molded with different curvatures (R = 4.5 mm, 5.5 mm, and 10 mm) in Stage II for practical applications. The shapes of the patterns are maintained without deformation (Fig. 5b). As shown in Fig. 5c, 5-μm-wide pillar and 2-μm-wide grating micropatterns that can maintain their shapes during the thermal treatment are successfully fabricated (Fig. S12). The intrinsic water contact angle (WCA) of the material is *ca.* 75° which is not affected by the thermal treatment (Fig. 5d). The modified material with pillar patterns on the surface has a WCA of up to 161° and is therefore hydrophobic. After thermal curing, this WCA value slightly increased from 161° to 169° (Fig. 5d). Meanwhile, grating patterns exhibit anisotropic hydrophobic properties. As shown in Fig. 5d, the patterned surface is hydrophilic with WCA at 59° when the droplet is placed parallel with the grating direction. On the contrary, this material shows superhydrophobicity with WCA at 140° when the droplet is perpendicular to the grating lines. This method offers a facile and convenient way to fabricate functional and curved microstructures, *e.g.* tools for microfluidic dynamic study.

4. Conclusions

In summary, a dual-curing polymer network based on sequential free radical polymerization and etherification was developed. The first polymerization step which is photoinitiated can be used for making sophisticated architectures using UV-based advanced manufacturing technologies. Two-dimensional (2D) and three-dimensional (3D) structures formed by the polymer networks in the first stage could be further programmed into other desired geometries. A subsequent thermally triggered curing step would render the new geometries permanent. Moreover, the mechanical performance of these materials is improved thanks to the generation of more densely crosslinked polymer networks. For example, depending on the material composition, the Young's modulus and glass transition temperature in Stage I range from 342 MPa to 1146 MPa and from 52 °C to 83 °C, respectively. After heating, the respective values range from 807 MPa to 1607 MPa and from 67 °C to 100 °C. By exploiting the advantages of the two curing steps, we could readily obtain rigid 2.5/3D structures by programming printed 2D sheets at relatively high temperatures. Also, 3D printed patterned microstructures from the proposed materials can be easily programmed into bent shapes with different curvatures, which may broaden the potential applications of such structures. Furthermore, micropatterned substrates created from the hydrophilic dual-stage crosslinked photopolymers by imprinting lithography exhibit superhydrophobicity. For practical applications, the as-fabricated flat substrates can be further molded with desired curvatures.

Declaration of Competing Interest

The authors declare that they have no known competing financial interests or personal relationships that could have appeared to influence the work reported in this paper.

Acknowledgements

B.Z. acknowledges Science, Technology and Innovation Commission of Shenzhen Municipality (no. JCYJ20190806152601638) and the National Natural Science Foundation of China (No. 51903210). H.L. acknowledges the support provided by China Scholarship Council (CSC) for his study at SUTD (CSC201806130090). Q.G. acknowledges the Key-Area Research and Development Program of Guangdong Province (Grant No.: 2020B090923003), and the support by the Centers for Mechanical Engineering Research and Education at MIT and SUSTech. We also acknowledge support of the SUTD Digital Manufacturing and Design Center (DManD) for access to experimental and computational facilities.

Appendix A. Supplementary data

Supplementary data to this article can be found online at https://doi.org/10.1016/j.cej.2021.128466.

References

[1] E. Andrzejewska, Photopolymerization kinetics of multifunctional monomers, Prog. Polym. Sci. 26 (4) (2001) 605–665, https://doi.org/10.1016/S0079-6700(01)00004-1.
[2] E. Blasco, M. Wegener, C. Barner-Kowollik, Photochemically driven polymeric network formation: synthesis and applications, Adv. Mater. 29 (2017) 1606000.
[3] C. Decker, Photoinitiated crosslinking polymerisation, Prog. Polym. Sci. 21 (4) (1996) 593–650, https://doi.org/10.1016/0079-6700(95)00027-5.
[4] J. Fouassier, J. Lalevée, Photochemical production of interpenetrating polymer networks; simultaneous initiation of radical and cationic polymerization reactions, Polymers 6 (10) (2014) 2588–2610, https://doi.org/10.3390/polym6102588.
[5] K.S. Anseth, S.M. Newman, C.N. Bowman, Polymeric dental composites: properties and reaction behavior of multimethacrylate dental restorations, Adv. Polym. Sci. 122 (1995) 177–217.
[6] D. Seliktar, Designing cell-compatible hydrogels for biomedical applications, Science 336 (6085) (2012) 1124–1128, https://doi.org/10.1126/science:1214804.
[7] J. Torgersen, X.-H. Qin, Z. Li, A. Ovsianikov, R. Liska, J. Stampfl, Hydrogels for two-photon polymerization: a toolbox for mimicking the extracellular matrix, Adv. Funct. Mater. 23 (2013) 4542–4554.
[8] B. Zhang, S. Li, H. Hingorani, A. Serjouei, L. Larush, A.A. Pawar, W.H. Goh, A. H. Sakhaei, M. Hashimoto, K. Kowsari, S. Magdassi, Q.i. Ge, Highly stretchable hydrogels for UV curing based high-resolution multimaterial 3D printing, J. Mater. Chem. B 6 (20) (2018) 3246–3253, https://doi.org/10.1039/C8TB00673C.
[9] H. Ben youcef, O. Garcia-Calvo, N. Lago, S. Devaraj, M. Armand, Cross-linked solid polymer electrolyte for all-solid-state rechargeable lithium batteries, Electrochim. Acta 220 (2016) 587–594, https://doi.org/10.1016/j.electacta.2016.10.122.
[10] D.P. Nair, N.B. Cramer, J.C. Gaipa, M.K. McBride, E.M. Matherly, R.R. McLeod, R. Shandas, C.N. Bowman, Two-stage reactive polymer network forming systems, Adv. Funct. Mater. 22 (7) (2012) 1502–1510, https://doi.org/10.1002/adfm.201102742.
[11] M.G. Hennessy, A. Vitale, O.K. Matar, J.T. Cabral, Controlling frontal photopolymerization with optical attenuation and mass diffusion, Phys. Rev. E 91 (6) (2015), https://doi.org/10.1103/PhysRevE.91.062402.
[12] T.M. Roper, T. Kwee, T.Y. Lee, C.A. Guymon, C.E. Hoyle, Photopolymerization of pigmented thiol–ene systems, Polymer 45 (9) (2004) 2921–2929, https://doi.org/10.1016/j.polymer.2004.02.038.
[13] Z. Yang, D.A. Wicks, C.E. Hoyle, H. Pu, J. Yuan, D. Wan, Y. Liu, Newly UV-curable polyurethane coatings prepared by multifunctional thiol- and ene-terminated polyurethane aqueous dispersions mixtures: Preparation and characterization, Polymer 50 (2009) 1717–1722.
[14] J. Dai, S. Ma, Y. Wu, J. Zhu, X. Liu, High bio-based content waterborne UV-curable coatings with excellent adhesion and flexibility, Prog. Org. Coat. 87 (2015) 197–203, https://doi.org/10.1016/j.porgcoat.2015.05.030.
[15] J. Oh, M. Seo, Photoinitiated polymerization-induced microphase separation for the preparation of nanoporous polymer films, ACS Macro Lett. 4 (11) (2015) 1244–1248, https://doi.org/10.1021/acsmacrolett.5b00734.
[16] E.C. Hagberg, M. Malkoch, Y. Ling, C.J. Hawker, K.R. Carter, Effects of modulus and surface chemistry of thiol-ene photopolymers in nanoimprinting, Nano Lett. 7 (2) (2007) 233–237, https://doi.org/10.1021/nl061217f.s001.
[17] C.J. Kloxin, T.F. Scott, H.Y. Park, C.N. Bowman, Mechanophotopatterning on a photoresponsive elastomer, Adv. Mater. 23 (17) (2011) 1977–1981, https://doi.org/10.1002/adma.201100323.
[18] D.K. Patel, A.H. Sakhaei, M. Layani, B. Zhang, Q. Ge, S. Magdassi, Highly stretchable and UV curable elastomers for digital light processing based 3D printing, Adv. Mater. 29 (2017) 1606000.
[19] Q. Ge, A.H. Sakhaei, H. Lee, C.K. Dunn, N.X. Fang, M.L. Dunn, Multimaterial 4D printing with tailorable shape memory polymers, Sci. Rep. 6 (2016) 31110.
[20] X. Fernández-Francos, A.-O. Konuray, A. Belmonte, S. De la Flor, À. Serra, X. Ramis, Sequential curing of off-stoichiometric thiol–epoxy thermosets with a custom-tailored structure, Polym. Chem. 7 (12) (2016) 2280–2290, https://doi.org/10.1039/C6PY00099A.
[21] G. González, X. Fernández-Francos, À. Serra, M. Sangermano, X. Ramis, Environmentally-friendly processing of thermosets by two-stage sequential aza-

Michael addition and free-radical polymerization of amine–acrylate mixtures, Polym. Chem. 6 (39) (2015) 6987–6997, https://doi.org/10.1039/C5PY00906E.
[22] D.P. Nair, N.B. Cramer, M.K. McBride, J.C. Gaipa, R. Shandas, C.N. Bowman, Enhanced two-stage reactive polymer network forming systems, Polymer 53 (12) (2012) 2429–2434, https://doi.org/10.1016/j.polymer.2012.04.007.
[23] H. Peng, D.P. Nair, B.A. Kowalski, W. Xi, T. Gong, C. Wang, M. Cole, N.B. Cramer, X. Xie, R.R. McLeod, C.N. Bowman, High performance graded rainbow holograms via two-stage sequential orthogonal thiol–click chemistry, Macromolecules 47 (7) (2014) 2306–2315, https://doi.org/10.1021/ma500167x.
[24] C.M. Yakacki, M. Saed, D.P. Nair, T. Gong, S.M. Reed, C.N. Bowman, Tailorable and programmable liquid-crystalline elastomers using a two-stage thiol–acrylate reaction, RSC Adv. 5 (25) (2015) 18997–19001, https://doi.org/10.1039/C5RA01039J.
[25] M. Retailleau, A. Ibrahim, C. Croutxé-Barghorn, X. Allonas, C. Ley, D. Le Nouen, One-pot three-step polymerization system using double click michael addition and radical photopolymerization, ACS Macro Lett. 4 (12) (2015) 1327–1331, https://doi.org/10.1021/acsmacrolett.5b00675.s001.
[26] M. Flores, A.M. Tomuta, X. Fernández-Francos, X. Ramis, M. Sangermano, A. Serra, A new two-stage curing system: thiol-ene/epoxy homopolymerization using an allyl terminated hyperbranched polyester as reactive modifier, Polymer 54 (2013) 5473–5481.
[27] D. Foix, X. Ramis, A. Serra, M. Sangermano, UV generation of a multifunctional hyperbranched thermal crosslinker to cure epoxy resins, Polymer 52 (15) (2011) 3269–3276, https://doi.org/10.1016/j.polymer.2011.05.029.
[28] S.C. Ligon-Auer, M. Schwentenwein, C. Gorsche, J. Stampfl, R. Liska, Toughening of photo-curable polymer networks: a review, Polym. Chem. 7 (2) (2016) 257–286, https://doi.org/10.1039/C5PY01631B.
[29] R.A. Ortiz, B.A.P. Urbina, L.V.C. Valdez, L.B. Duarte, R.G. Santos, A.E.G. Valdez, M. D. Soucek, Effect of introducing a cationic system into a thiol-ene photopolymerizable formulation, J. Polym. Sci. A Polym. Chem. 45 (21) (2007) 4829–4843, https://doi.org/10.1002/pola.22234.
[30] M. Sangermano, M. Cerrone, G. Colucci, I. Roppolo, R.A. Ortiz, Preparation and characterization of hybrid thiol-ene/epoxy UV–thermal dual-cured systems, Polym. Int. 59 (2010) 1046–1051.
[31] G. Griffini, M. Invernizzi, M. Levi, G. Natale, G. Postiglione, S. Turri, 3D-printable CFR polymer composites with dual-cure sequential IPNs, Polymer 91 (2016) 174–179, https://doi.org/10.1016/j.polymer.2016.03.048.
[32] J. Cushen, J. Goodrich, J.P. Rolland, Epoxy dual cure resins for additive manufacturing, 2016.
[33] X. Kuang, Z. Zhao, K. Chen, D. Fang, G. Kang, H.J. Qi, High-speed 3D printing of high-performance thermosetting polymers via two-stage curing, Macromol. Rapid Commun. 39 (2018) 1700809.
[34] J.J. Weigand, C.I. Miller, A.P. Janisse, O.D. McNair, K. Kim, J.S. Wiggins, 3D printing of dual-cure benzoxazine networks, Polymer 189 (2020), 122193.
[35] T. Wu, P. Jiang, Z. Ji, Y. Guo, X. Wang, F. Zhou, W. Liu, 3D printing of high-performance isocyanate ester thermosets, Macromol. Mater. Eng. 305 (2020) 2000397.
[36] Y. Cui, J. Yang, D. Lei, J. Su, 3D printing of a dual-curing resin with cationic curable vegetable oil, Ind. Eng. Chem. Res. 59 (25) (2020) 11381–11388, https://doi.org/10.1021/acs.iecr.0c01507.s001.
[37] O. Konuray, F. Di Donato, M. Sangermano, J. Bonada, A. Tercjak, X. Fernandez-Francos, A. Serra, X. Ramis, Dual-curable stereolithography resins for superior thermomechanical properties, eXPRESS Polym. Lett. 14 (9) (2020) 881–894, https://doi.org/10.3144/expresspolymlett.2020.72.
[38] C. Lu, C. Wang, J. Yu, J. Wang, F. Chu, Two-step 3 D-printing approach toward sustainable, repairable, fluorescent shape-memory thermosets derived from cellulose and rosin, ChemSusChem 13 (2020) 854.
[39] R. Yu, X. Yang, Y. Zhang, X. Zhao, X. Wu, T. Zhao, Y. Zhao, W. Huang, Three-dimensional printing of shape memory composites with epoxy-acrylate hybrid photopolymer, ACS Appl. Mater. Interfaces 9 (2) (2017) 1820–1829, https://doi.org/10.1021/acsami.6b13531.s002.
[40] B. Zhang, K. Kowsari, A. Serjouei, M.L. Dunn, Q. Ge, Reprocessable thermosets for sustainable three-dimensional printing, Nat. Commun. 9 (2018) 1831.
[41] Q. Ge, Z. Li, Z. Wang, K. Kowsari, W. Zhang, X. He, J. Zhou, N.X. Fang, Projection micro stereolithography based 3D printing and its applications, Int. J. Extrem. Manuf. 2 (2020), 022004.
[42] J.R. Tumbleston, D. Shirvanyants, N. Ermoshkin, R. Janusziewicz, A.R. Johnson, D. Kelly, K. Chen, R. Pinschmidt, J.P. Rolland, A. Ermoshkin, E.T. Samulski, J. M. DeSimone, Continuous liquid interface production of 3D objects, Science 347 (6228) (2015) 1349–1352, https://doi.org/10.1126/science:aaa2397.
[43] X. Zheng, J. Deotte, M.P. Alonso, G.R. Farquar, T.H. Weisgraber, S. Gemberling, H. Lee, N. Fang, C.M. Spadaccini, Design and optimization of a light-emitting diode projection micro-stereolithography three-dimensional manufacturing system, Rev. Sci. Instrum. 83 (2012), 125001.
[44] T. Kaiser, Highly crosslinked polymers, Prog. Polym. Sci. 14 (3) (1989) 373–450, https://doi.org/10.1016/0079-6700(89)90007-5.
[45] E.A. Campo, in: Selection of Polymeric Materials, Elsevier, 2008, pp. 103–140, https://doi.org/10.1016/B978-081551551-7.50005-X.
[46] P.R. Couchman, Compositional variation of glass-transition temperatures. 2. Application of the thermodynamic theory to compatible polymer blends, Macromolecules 11 (6) (1978) 1156–1161, https://doi.org/10.1021/ma60066a018.
[47] J. Wu, Z. Zhao, C.M. Hamel, X. Mu, X. Kuang, Z. Guo, H.J. Qi, Evolution of material properties during free radical photopolymerization, J. Mech. Phys. Solids 112 (2018) 25–49, https://doi.org/10.1016/j.jmps.2017.11.018.
[48] H. Stutz, K.-H. Illers, J. Mertes, A generalized theory for the glass transition temperature of crosslinked and uncrosslinked polymers, J. Polym. Sci. B Polym. Phys. 28 (9) (1990) 1483–1498, https://doi.org/10.1002/polb.1990.090280906.
[49] A.T. DiBenedetto, Prediction of the glass transition temperature of polymers: a model based on the principle of corresponding states, J. Polym. Sci. B Polym. Phys. 25 (9) (1987) 1949–1969, https://doi.org/10.1002/polb.1987.090250914.
[50] K. Yu, Q. Ge, H.J. Qi, Reduced time as a unified parameter determining fixity and free recovery of shape memory polymers, Nat. Commun. 5 (2014) 3066.
[51] S. Waheed, J.M. Cabot, N.P. Macdonald, T. Lewis, R.M. Guijt, B. Paull, M. C. Breadmore, 3D printed microfluidic devices: enablers and barriers, Lab. Chip 16 (11) (2016) 1993–2013, https://doi.org/10.1039/C6LC00284F.
[52] K. Liu, X.i. Yao, L. Jiang, Recent developments in bio-inspired special wettability, Chem. Soc. Rev. 39 (8) (2010) 3240, https://doi.org/10.1039/b917112f.
[53] W.L. Lee, H.Y. Low, Geometry- and length scale-dependent deformation and recovery on micro- and nanopatterned shape memory polymer surfaces, Sci. Rep. 6 (1) (2016), https://doi.org/10.1038/srep23686.
[54] S.H. Lim, H.Y. Low, W.S. Tan, Novel soft stamp development for direct micro- and nano-patterning of macroscopic curved surfaces, J. Vac. Sci. Technol. B 34 (2016) 11602.
[55] J.Y. Quek, C.L. Magee, H.Y. Low, Physical texturing for superhydrophobic polymeric surfaces: a design perspective, Langmuir 33 (2017) 6902–6915.
[56] X.J. Feng, L. Jiang, Design and creation of superwetting/antiwetting surfaces, Adv. Mater. 18 (23) (2006) 3063–3078, https://doi.org/10.1002/adma.200501961.
[57] K. Liu, L. Jiang, Bio-inspired self-cleaning surfaces, Annu. Rev. Mater. Res. 42 (1) (2012) 231–263, https://doi.org/10.1146/annurev-matsci-070511-155046.
[58] D. Wu, S.-Z. Wu, Q.-D. Chen, Y.-L. Zhang, J. Yao, X.i. Yao, L.-G. Niu, J.-N. Wang, L. Jiang, H.-B. Sun, Curvature-driven reversible in situ switching between pinned and roll-down superhydrophobic states for water droplet transportation, Adv. Mater. 23 (4) (2011) 545–549, https://doi.org/10.1002/adma.201001688.
[59] E. Kizilkan, S.N. Gorb, Combined effect of the microstructure and underlying surface curvature on the performance of biomimetic adhesives, Adv. Mater. 30 (2018) 1704696.
[60] W.L. Lee, D. Wang, J. Wu, Q.i. Ge, H.Y. Low, Injection molding of superhydrophobic submicrometer surface topography on macroscopically curved objects: experimental and simulation studies, ACS Appl. Polym. Mater. 1 (6) (2019) 1547–1558, https://doi.org/10.1021/acsapm.9b00312.s001.